Nanostructured fusiform hydroxyapatite particles precipitated from aquaculture wastewater

Covadonga Correas,[a] Michael L. Gerardo,[b,‡] Alexander M. Lord,[c] Michael B. Ward,[d] Enrico Andreoli,*[a] Andrew R. Barron*[a,e,f]

[a] *Energy Safety Research Institute, Swansea University, Bay Campus, Swansea, SA1 8QQ, Wales, UK.*
[b] *College of Engineering, Swansea University, Bay Campus, Swansea, SA1 8QQ, Wales, UK.*
[c] *Centre for NanoHealth, Swansea University, Singleton Campus, SA2 8PP, Wales, UK.*
[d] *Leeds Electron Microscopy and Spectroscopy Centre, University of Leeds, LS2 9JT, England, UK.*
[e] *Department of Chemistry, Rice University, Houston, Texas 77005, USA.*
[f] *Department of Materials Science and Nanoengineering, Rice University, Houston, TX 77005, USA.*

HIGHLIGHTS

- HAp precipitated from aquaculture wastewater using mild-methods.
- Fusiform shape and nano size only previously been achieved by synthetic routes.
- Phosphate recovery does not require the addition of seed chemicals.
- Ca:P ratios (1.21-1.44) are lower than that usually observed for HAp (1.67).

Keywords hydroxyapatite; trout; calcium phosphate; morphology; nano; fusiform

‡ Present address: Dwr Cymru Welsh Water, Dinas Depot, Lanwnda, Caernarfon, LL54 5UD Wales, UK.
* Corresponding authors. E-mail: e.andreoli@swansea.ac.uk (E. Andreoli). a.r.barron@swansea.ac.uk; arb@rice.edu (A. R. Barron).

ABSTRACT

The present work represents a new approach for the isolation of uniform nano particulate hydroxyapatite (HAp). The chemical characterization of a calcium phosphate product obtained from industrial trout farm aquaculture wastewater by two different routes, washing either with a basic aqueous medium ($wash_{NaOH}$) or followed by a further washing with ethanol ($wash_{EtOH}$), is explored. Characterization of the isolated materials includes morphology studies (SEM and TEM), structural (XRD, electron diffraction), compositional (EDX) and thermogravimetric analysis (TGA). The obtained products are a mixture of different compounds, with hydroxyapatite the predominant phase. The morphology is unusually nanometric size with fusiform shaped particles, such characteristics are ordinarily only obtained by synthetic routes. This process of phosphate precipitation represents a unique self-sufficient process to be compared to conventional chemical or biological practices for precipitating phosphate.

1. Introduction

Calcium phosphate based materials are used in numerous applications such as fertilizers (Ferraro, et al., 2013), environmental remediation of waters and soils (Nzihou and Sharrock, 2010; Piccirillo et al., 2013), photocatalysis (Tanaka et al., 2012; Piccirillo et al, 2013) and as biomaterials (Vallet-Regí, 2010; Dorozhkin, 2010; Kim, 2011; Zhou and Lee, 2011). Interestingly, one of these compounds, hydroxyapatite [HAp, $Ca_{10}(PO_4)_6(OH)_2$] is commonly used as a bioceramic, due to its osteoconductivity and high biocompatibility properties. HAp also has the ability to promote the formation of new bone tissues, making it a perfect material as a support or filler in bones and teeth (Vallet-Regí, 2010; Kim, 2011; Zhou and Lee, 2011).

HAp for biomaterials is normally obtained by a range synthetic routes including: electrophoretic deposition and microwave assisted hydrothermal treatment (Hayek et al., 1963; Dorozhkin, 2010; Weiner and Addadi, 2011). The structure, morphology, and composition of the product are dependent on the method employed, resulting in some limitations in structural morphology for synthetic HAp (Zhou and Lee, 2011). As an alternative, the extraction of natural HAp from animals has been proposed, based on the more

favorable properties and high percentage weight of HAp found in bones. Extraction of natural HAp from residue of eggshells, seashells, starfishes or animal bones has been successfully described in the literature (Rocha et al., 2005; Ozawa and Suzuki, 2002; Mondal et all, 2010; Bardhan et al., 2011; Akram et al., 2014). These practices have important considerations, owing to the possibility to obtain large amounts of HAp, and also the potential role in waste management in industry, e.g., reduction of solids, calcium and phosphate in waste streams. The more typical approach to phosphate removal is through chemical crystallization of HAp by the addition of a seed crystal or additives (de-Bashan and Bashan, 2004; Bellier et al., 2006; Song et al., 2006; Zhang et al., 2007; Chen et al., 2009;).

Aquaculture wastewaters are particularly rich in calcium and phosphate, which are mostly trapped within the wastewater sediment (Seawright et al., 1998). Alkaline heat treatment has been previously described (Sankar et al., 2008; Panda et al., 2014] for the extraction of natural HAp from fish scales. More recently, in an attempt to develop mild methodologies of natural HAp from aquaculture wastewater, we have demonstrated that simple pH adjustment and membrane filtration leads to the recovery of calcium phosphate minerals from trout farm wastewater sediment (Gerardo et al., 2015). Whilst it was argued that the presence of calcium phosphate minerals was related to undigested feed found in the sediment, i.e., fish bones and fish scales, the characterization of the calcium apatite mineral was not carried out. Herein we report the chemical and structural characterization of calcium phosphate minerals obtained from industrial trout farm aquaculture wastewater.

2. Materials and methods

2.1. Processing

Industrial trout wastewater was obtained from a solids-settling tank from a fish farm located in England, Romsey. The wastewater was adjusted to pH 3 using 1 M HCl (Fisher Scientific, UK) and allowed to set over a period of 24 hours. Subsequently, the supernatant was sieved through a 500 μm mesh and filtered using a hollow fiber membrane cartridge with 0.2 μm pore size (polysulphone, AGT, UK) setup on a benchtop filtration apparatus (AGT Quix Stand, UK). The permeate obtained was adjusted to pH 8 using 1 M NaOH (Fisher Scientific,

UK) to give a precipitate that was centrifuged at 9000 rpm for 10 minutes. The yield of precipitation was 99.1 %.

The supernatant was discarded and two separate washing methodologies were applied to the precipitates by replacing an equal volume of the supernatant: 1) deionized H_2O followed by 1 M NaOH and 2) deionized H_2O followed by 1 M NaOH followed by ethanol ($wash_{EtOH}$, 99.5 % absolute analytical reagent grade from Fisher Scientific). Between each one of the steps for each one of the methodologies, the precipitate was re-suspended using a vortex mixer. Thereafter, centrifuged at 9000 rpm for 10 minutes, all wash solutions were discarded and a final pellet was obtained and transferred to a petri dish. A control sample ($wash_{control}$) was carried out by not washing the precipitate. The washing procedures were carried out three times and the final precipitate was dried at 105 °C.

2.2. Characterization

The phase identification of the products was investigated by XRD using a Bruker AXS D8 Advance diffractometer with an LINXEYE detector between 10° and 70° (2θ), with 2θ increments of 0.05° and counting time of 1.5 s. The Cu-K_α (λ = 1.5418 Å) was used in these experiments. Further characterization was carried out by IR analysis of all the samples, Thermoscientific i510 FTIR equipment was used; recording spectra in the 650-4000 cm^{-1} region with 16 scans. The morphology of the samples was examined by field emission scanning electron microscopy with an Ultra-High Resolution FE-SEM Hitachi S-4800, equipped with an Inca electron dispersive X-ray detector (Oxford Instruments, Abingdon, United Kingdom) for EDX experiments. The samples were also characterized by transmission electron microscopy, using a Tecnai F20 200 kV FEGTEM fitted with a Gatan SC600 CCD camera used to record both images and diffraction patterns, for EDX an Oxford Instrument Xmax 80 mm^2 SDD was used. 200 particles were measured from TEM images for the average particle sizes. Thermogravimetric analysis (TGA) of the samples were performed on a Q600 TA instrument, under flowing air (100 mL/min) from room temperature to 1300 °C with a heating rate of 20 °C/min. $Wash_{NaOH}$ and $wash_{EtOH}$ samples were also heated at 1200 °C for one hour. After the heating, both samples were characterized by XRD and FTIR.

3. Results and discussion

The morphology of the nanoparticulate present in the precipitated material is similar irrespective of the washing being performed and the washing solutions used ($wash_{control}$, $wash_{NaOH}$ or $wash_{EtOH}$). The typical morphology is shown in the SEM (Fig. 1a) of the precipitate obtained from the EtOH treatment ($wash_{EtOH}$). This morphology can be described as an agglomeration of rod or fusiform shapes (tapering at both ends) into a hierarchical structure. This is interesting since, while natural HAp has been reported to assume many different shapes such as fibers (Aizawa et al., 2006), spheres (Dědourková et al., 2012; Kamitakahara et al., 2013), needles (Cengiz et al., 2008) or even amorphous (Mobasherpour et al., 2007), it has not been reported with fusiform shapes. Thus, this precipitation from a biological source allows for a broadening of available morphologies to be used.

When the samples were observed by TEM (Fig. 1b), it was possible to see that these rods were formed of nanoparticles aggregated into elongated structures. Similar pseudo-one dimensional aggregates have been previously reported for a range of nanoparticles, even when spherical (Stoll et al., 1996). The material from the EtOH treatment has an average particle length of 28 nm, with a distribution shown in Fig. 2. Such nanoparticle structures have been previously described for synthetic nanocrystalline HAp (Mobasherpour et al., 2007). Thus, it is possible to obtain nanostructured fusiform hydroxyapatite particles with the use of these precipitation and washing methods rather than having to synthesize material.

The results of the EDX analysis of the solids obtained after the different washing procedures are shown in Table 1. The $wash_{EtOH}$ sample is composed entirely of Ca, P, O, and C. While these elements comprise ca. 97% of the $wash_{Control}$ and $wash_{NaOH}$ samples, small amounts of Na and Cl were detected in the former, and Si is detected in the latter. The absence of these elements in the $wash_{EtOH}$ sample was also confirmed by TEM-EDX (Fig. 3), although some traces of Cu were observed due to the Cu TEM grid that the sample was mounted on. The presence of salt in the $wash_{Control}$ sample is possibly due to contamination from acidification and alkalinization treatments. While, there is no obvious explanation for the presence of Si in the $wash_{NaOH}$ sample, but given the low concentration, it may be interpreted as result of etching the glass container. We also note that the ethanol washing

favors a reduction in the carbon content in the isolated sample, probably due to the elimination of organic matter. This is consistent with the synergetic effects between the NaOH and EtOH for the removal of membrane foulants (Tian et al., 2010).

Based on EDX analyses (Table 1) the Ca:P ratios for the samples is in the 1.21-1.44, which is lower than that usually observed for HAp (Ca:P ratio of 1.67) (Elliott, 2002; Dorozhkin, 2013). Although it is not possible to determine the crystallographic structure of the precipitates based on EDX, the results show a similar composition to that described for carbonated Ca-deficient HAp (see below). As such, this is particularly interesting since calcium phosphate highly substituted with carbonate is a composing mineral of human teeth and bones (Featherstone and Lussi, 2006; Dorozhkin, 2013). Low Ca:P ratios have been correlated with the presence of $[HPO_4]^{2-}$ ions formed under acidic conditions (Combes and Rey, 2010). The specific formation of calcium-deficient HAp undergoes a transitional stage as composed of octocalcium phosphate. According to previous work, pure HAp can be synthesized from calcium-deficient HAp by adjusting reaction temperature and time at pH 10-11 and Ca^{2+} ion concentrations to values higher than 0.5 mol/L (Liu et al., 2001).

XRD measurements of the samples were carried out in order to determine the crystalline phases and structures of the products after precipitation and washing. Fig. 4 shows the XRD patterns of the samples, in which very broad peaks are observed, due to the nanometric size of the particles and the presence of amorphous phases formed during the precipitation. In spite of that, it is possible to identify a main phases composed of hydroxyapatite (JPDF card no. 9014313). Minor constituents may be characterized as portlandite (JPDF card no. 9006836) and aragonite (JPDF card no. 9015149). Although indications that they are present in both samples, they are more readily differentiated in the $wash_{NaOH}$ samples. Despite being a metastable phase, aragonite is commonly formed in biological samples, especially those in marine and freshwater environments, and as such is expected; however, portlandite is a mineral form and not usually associated with biological material.

An estimation of the particle size may be calculated from the XRD pattern for the samples washed with NaOH ($wash_{NaOH}$) using the Debye-Scherrer equation using the (211)

peak, from which a crystallite diameter of 16 nm is determined. This value is in good agreement with high-resolution TEM images (Fig. 5a). From the TEM images it is possible to distinguish the alignment of the crystal planes, which indicates the high crystallinity of the sample at the nano-scale. The electron diffraction patterns of the particles supported the presence of hydroxyapatite in the sample, because it is possible to correlate the rings obtained in measurement with the HAp crystal planes [002], [3-21], [4-10], [4-22] and [004], see Fig. 5b.

FTIR measurements corroborated the presence of hydroxyapatite and aragonite in the sample. Fig. 6 shows the FTIR spectrum for the sample obtained through EtOH treatment ($wash_{EtOH}$). A weak band for OH-groups is found at 3570 cm^{-1} (stretching vibration). The weakness of the band would suggest pore crystallization; however, similarly weak bands have been observed previously for crystalline HAp (Panda et al., 2003; Avés et al., 2007; Luis et al., 2012). The typical band vibration mode for HO^- is not seen at 630 cm^{-1}, possibly overlapped by the ν_4 bands of $[PO_4]^{3-}$ at 600 and 560 cm^{-1} (Gibson et al., 2000; Hutchens et al., 2006]. Such a weak hydroxide band is also commonly found in bone minerals, but a broad water band at 3400 cm^{-1} normally obscures its detection. In this case the water band is weak and slightly shifted to ca. 3300 cm^{-1}; allowing for the hydroxide band to show. Since the mineral sample was dried in the oven at 100 °C, this suggests that the mineral has the ability to bind water. Theoretically, there are four vibrational modes present for phosphate ions and these are labeled in the FTIR spectrum shown in Fig. 6. A very strong ν_3 band is identified at 1027 cm^{-1}, which has obscured another common ν_3 band at 1090 cm^{-1} (only slightly visible). This strong $[PO_4]^{3-}$ ν_3 band can also overlap with the $[CO_3]^{2-}$ band. These specific wavenumbers for the phosphate ν_3 band at 1027 and 1090 cm^{-1} are typical of Ca-deficient HAp. In addition, the $[HPO_4]^{2-}$ band at 2200-2000 cm^{-1} is typically of Ca-deficient HAp (Gibson et al., 2000; Hutchens et al., 2006). The phosphate ν_1 and ν_2 bands are present at 970 cm^{-1} and 475 cm^{-1}, respectively. Finally, the presence of aragonite is suggested by the three bands at 1650, 1454 and 1413 cm^{-1} $[CO_3]^{2-}$ ν_3; and, one ν_2 band at ca. 870 cm^{-1}. The bands assignments in agreement with literature data (Fenner, 1913; Rey et al., 1995; Ślósarczyk et al., 2005).

In order to increase the particle size and to know more about the crystallographic phases present, a thermal annealing study was carried out. The TGA analysis (Fig. 7) showed a similar thermal behavior for both samples ($wash_{EtOH}$ and $wash_{NaOH}$). In general, a higher weight loss is observed in the $wash_{NaOH}$ sample, probably due to the presence of a higher amount of organic compounds, which are decomposed with the heating. Two similar weight drops related with water losses are observed in the TGA curves for both samples: from 50 to 150 °C, the adsorbed water is evaporated and from 250 to 400 °C, the loss of more adsorbed and lattice water is observed. Around 450-800 °C a similar weight loss appears in both samples. As described later in the XRD studies, the formation of quartz during the heating could be possible in this range of temperatures. The main differences are shown in the region >800 °C, where a significant weight loss occurs for the $wash_{NaOH}$ sample, but a weight increase appears in the $wash_{EtOH}$ sample. In the case of $wash_{NaOH}$ the loss is attributed to the $[CO_3]^{2-}$ decomposition. In contrast, the weight increase in the $wash_{EtOH}$ sample seems to be due to the formation of a new oxidized phase, which could not be identified (see below).

XRD measurements of the samples heated to 1200 °C revealed the occurrence of a series of phase transformations (Fig. 8). In both cases a mix of different phases appeared. Upon annealing the hydroxyapatite in the $wash_{NaOH}$ sample increases in crystallinity (i.e., Fig. 8 versus Fig. 4). In addition, it is possible to characterize β-tricalcium phosphate (bone phosphate of lime, $Ca_3(PO_4)_2$, JPDF card no. 1517238), CaO (JPDF card no. 9006713), and quartz (JPDF card no. 9010144). The CaO is obtained through aragonite decomposition, while the quartz is due to crystallization of the amorphous silica observed in the original sample. These phases are in agreement with the TGA results. The annealing of the $wash_{EtOH}$ sample also forms hydroxyapatite, bone phosphate of lime, and quartz. The SiO_2 polymorphs crystalize at 573 and 870 °C, respectively and can be obtained with rapid cooling (Conejero et al., 2006). In the $wash_{EtOH}$ sample there is no evidences of CaO formation.

4. Conclusions

This work demonstrates the possibility of precipitating HAp using mild-methods to produce a defined particle shape and nano size that has only previously been achieved by synthetic

routes. One of the benefits to the sustainable recovery of phosphate described herein is that the method reported in this work requires only pH change for precipitation followed by washing. In particular, unlike other reports, this process does not necessitate the use of seed materials (Song et al., 2006; Zhang et al., 2007). This process of phosphate precipitation is in fact a self-sufficient one and as such this represents a unique process considering the conventional practices in precipitating phosphate, using coagulants (Clark et al., 2000; Gaterell et al., 2000), via chemical precipitation (Çelen and Türker, 2001; Song et al., 2006; Shu et al., 2006; Zhang et al., 2007; Türker and Çelen, 2007), and biological removal of phosphate (Oehmen et al., 2005). We acknowledge that if this material were to be used for surgery or orthopaedic application, careful removal of unknown substances would be necessary; however, the ability to have an almost unlimited source could outweigh the further purification that may be needed.

Acknowledgments

Financial support was provided by the Welsh Government Sêr Cymru Programme and the Robert A. Welch Foundation (C-0002). TEM characterization data was enabled via support from the EPSRC-funded Leeds EPSRC Nanoscience and Nanotechnology Equipment Facility (LENNF) (EP/K023853/1). The authors declare no competing financial interests.

References

Aizawa, M., Ueno, H., Itatani, K., Okada, I., 2006. Syntheses of calcium-deficient apatite fibres by a homogeneous precipitation method and their characterizations. J. Eu. Ceram. Soc. 26, 501-507.

Akram, M., Ahmed, R., Shakir, I., Ibrahim, W.A.W., Hussain, R., 2014. Preparation of natural hydroxyapatite from bovine femur bones using calcination at various temperatures, J. Mater. Sci. 49, 1461-1475.

Avés, E.P., Sader, M.S., Jerônimo, F.A.R., Sena, L.A., Sierra, J.C.G., Soares, G.A., 2007. Comparative study of hydroxyapatite coatings obtained by sol-gel and electrophoresis on titanium sheets. Revista Matéria 12, 156-163.

Bardhan, R., Mahata, S., Mondal, B., 2011. Processing of natural resourced hydroxyapatite from eggshell waste by wet precipitation method. Adv. Appl. Ceram. 110, 80-86.

Bellier, N., Chazarenc, F., Comeau, Y., 2006. Phosphorus removal from wastewater by mineral apatite, Water Res. 40, 2965-2971.

Çelen, I., Türker, M., 2001. Recovery of ammonia as struvite from aneorobic digester effluents. Environ. Tech. 22, 1263-1272.

Cengiz, B., Gokce, Y., Yildiz, N., Aktas, Z., Calimli, A., 2008. Synthesis and characterization of hydroxyapatite nanoparticle. Colloid. Surface. A 322, 29-33.

Chen, X., Kong, H., Wu, D., Wang, X., Lin, Y., 2009. Phosphate removal and recovery through crystallization of hydroxyapatite using xonotlite as seed crystal, J. Environ. Sci. 21, 575-580.

Clark, T., Burgess, J., Stephenson, T., Arnold-Smith, A., 2000. Influence of iron-based co-precipitants on activated sludge biomass. Process Saf. Environ. 78, 405-410.

Combes, C., Rey, C., 2010. Amorphous calcium phosphates: synthesis, properties and uses in biomaterials. Acta Biomater. 6, 3362-3378.

Conejero, S., Song, M., Martin, D., Canac, Y., Soleilhavoup, M., Bertrand, G., 2006. New synthetic routes to c-amino phosphorus ylides and their subsequent fragmentation into carbenes and phosphines. Chem.- Asian J. 1, 155-160.

de-Bashan, L.E., Bashan, Y., 2004. Recent advances in removing phosphorus from wastewater and its future use as fertilizer (1997-2003), Water Res. 38, 4222-4246.

Dědourková, T., Zelenka, J., Zelenková, M., Beneš, L., Svoboda, L., 2012. Synthesis of sphere-like nanoparticles of hydroxyapatite. Procedia Eng. 42, 1816-1821.

Dorozhkin, S.V., 2010. Bioceramics of calcium orthophosphates, Biomaterials 31, 1465-1485.

Dorozhkin, S.V., 2013. A detailed history of calcium orthophosphates from 1770s till 1950. Mater. Sci. Eng. C 33, 3085-3110.

Elliott, J.C., 2002. Calcium phosphate biominerals. Rev. Mineral. Geochem. 48, 427-453.

Featherstone, J., Lussi, A., 2006. Understanding the chemistry of dental erosion. Dent. Erosion 20, 66-76.

Ferraro, V., Carvalho, A. P., Piccirillo, C., Santos, M.M., Castro, P.M., Pintado, M.E., 2013. Extraction of high added value biological compounds from sardine, sardine-type fish and mackerel canning residues - a review. Mater. Sci. Eng. C 33, 3111-3120.

Gaterell, M., Gay, R., Wilson, R., Gochin, R., Lester, J., 2000. An economic and environmental evaluation of the opportunities for substituting phosphorus recovered from wastewater treatment works in existing UK fertiliser markets. Environ. Tech. 21, 1067-1084.

Gerardo, M.L., Lord, A.M., Lovitt, R.W., 2015. An investigation of pH mediated extraction and precipitation of phosphorus from sludge using microfiltration: processing and costs, Separ. Sci. Tech. 50, 2155-2163.

Gibson, I., Rehman, I., Best, S., Bonfield, W., 2000. Characterization of the transformation from calcium-deficient apatite to beta-tricalcium phosphate. J. Mater. Sci.- Mater. Med. 11, 799-804.

Fenner, A.N., 1913. The stability relations of the silica minerals. Am. J. Sci. 331-384.

Hayek, E., Newseley, H., Rumpel, M. L., 1963. Pentacalcium monohydroxyorthophosphate. Inorg. Synth. 7, 63-65.

Hutchens, S.A., Benson, R.S., Evans, B.R., O'Neill, H.M., Rawn, C.J., 2006. Biomimetic synthesis of calcium-deficient hydroxyapatite in a natural hydrogel. Biomaterials 27, 4661-4670.

Kamitakahara, M., Imai, R., Ioku, K. 2013. Preparation and evaluation of spherical Ca-deficient hydroxyapatite granules with controlled surface microstructure as drug carriers. Mater. Sci. Eng. C 33, 2446-2450.

Kim, S.Y., 2011. Surface-engineered hydroxyapatite nanocrystal/ poly(ε-caprolactone) hybrid scaffolds for bone tissue engineering, J. Appl. Polym. Sci. 121, 1921-1929.

Liu, C., Huang, Y., Shen, W., Cui, J., 2001. Kinetics of hydroxyapatite precipitation at pH 10 to 1. Biomaterials 22, 301-306.

Luis, C., Mendes, G.L., Ribeiro, C., Marques, C., 2012. In-situ hydroxyapatite synthesis: influence of collagen on its structural and morphological characteristic. Mater. Sci. Appl. 3, 580-586.

Mobasherpour, I., Heshajin, M.S., Kazemzadeh, A., Zakeri, M., 2007. Synthesis of nanocrystalline hydroxyapatite by using precipitation method. J. Alloy. Compd. 430, 330-333.

Mondal, S., Mahata, S., Kundu, S., Mondal, B., 2010. Processing of natural resourced hydroxyapatite from eggshell waste by wet precipitation method, Adv. Appl. Ceram. 109, 234-239.

Nzihou, A., Sharrock, P., 2010. Role of phosphate in the remediation and reuse of heavy metal polluted wastes and sites. Waste Biomass Valor. 1, 163-174.

Oehmen, A., Lemos, P.C., Carvalho, G., Yuan, Z., Keller, J., Blackall, L. L., Reis, M. A., 2007. Advances in enhanced biological phosphorus removal: From micro to macro scale. Water Res. 41, 2271-2300.

Ozawa, M., Suzuki, S., 2002. Microstructural Development of natural hydroxyapatite originated from fish-bone waste through heat treatment, J. Am. Ceram. Soc. 85, 1315-1317.

Panda, R.N., Hsieh, M.F., Chung, R.J., Chin, T.S., 2003. FTIR, XRD, SEM and solid state NMR investigations of carbonate-containing hydroxyapatite nano-particles synthesized by hydroxide-gel technique. J. Phys. Chem. Solids 64, 193-199.

Panda, N., Pramanik, K., Sukla, L., 2014. Extraction and characterization of biocompatible hydroxyapatite from fresh water fish scales for tissue engineering scaffold, Bioproc. Biosyst. Eng. 12, 2615-2615.

Piccirillo, C., Pereira, S., Marques, A.P., Pullar, R., Tobaldi, D., Pintado, M.E., Castro, P.M., 2013. Bacteria immobilisation on hydroxyapatite surface for heavy metals removal, J. Environ. Manage. 121, 87-95.

Piccirillo, C., Dunnill, C.W., Pullar, R.C., Tobaldi, D.M., Labrincha, J.A., Parkin, I.P., Pintado, M.M., Castro, P.M., 2013. Calcium phosphate-based materials of natural origin showing photocatalytic activity, J. Mater. Chem. A 1, 6452-6461.

Rey, C., Miquel, J., Facchini, L., Legrand, A., Glimcher, M., 1995. Hydroxyl groups in bone mineral. Bone 16, 583-586.

Rocha, J., Lemos, A., Kannan, S., Agathopoulos, S., Ferreira, J., 2005. Hydroxyapatite scaffolds hydrothermally grown from aragonitic cuttlefish bones, J. Mater. Chem. 15, 5007-5011.

Sankar, S., Sekar, S., Mohan, R., Rani, S., Sundaraseelan, J., Sastry, T., 2008. Preparation and partial characterization of collagen sheet from fish (Lates calcarifer) scales, Int. J. Biol. Macromol. 42, 6-9.

Seawright, D.E., Stickney, R.R., Walker, R.B., 1998. Nutrient dynamics in integrated aquaculture–hydroponics systems, Aquaculture, 160, 215-237.

Shu, L., Schneider, P., Jegatheesan, V., Johnson, J., 2006. An economic evaluation of phosphorus recovery as struvite from digester supernatant. Bioresource Tech. 97, 2211-2216.

Ślósarczyk, A., Paszkiewicz, Z., Paluszkiewicz, C., 2005. FTIR and XRD evaluation of carbonated hydroxyapatite powders synthesized by wet methods. J. Mol. Struct. 744, 657-661.

Song, Y., Weidler, P. G., Berg, U., Nüesch, R., Donnert, D., 2006. Calcite-seeded crystallization of calcium phosphate for phosphorus recovery, Chemosphere 63, 236-243.

Stoll, S.L., Gillan, E.G., Barron, A.R., 1996. Chemical vapor deposition of Gallium selenide and indium selenide nanoparticles. Chem. Vapor Deposition 2, 182-184.

Tanaka, H., Tsuda, E., Nishikawa, H., Fuji, M., 2012. FTIR studies of adsorption and photocatalytic decomposition under UV irradiation of dimethyl sulfide on calcium hydroxyapatite, Advanced Powder Technol. 23, 115-119.

Tian, J.Y., Chen, Z.I., Yang, Y.I., Liang, H., Nan, J., Li, G.-B., 2010. Consecutive chemical cleaning of fouled PVC membrane using NaOH and ethanol during ultrafiltration of river water. Water Res. 44, 59-68.

Türker, I., Çelen, I., 2007. Removal of ammonia as struvite from anaerobic digester effluents and recycling of magnesium and phosphate. Bioresource Tech. 98, 1529-1534.

Vallet-Regí, M., 2010. Evolution of bioceramics within the field of biomaterials, Comptes Rendus Chimie 13, 174-185.

Weiner, S., Addadi, L., 2011. Crystallization pathways in biomineralization, Ann. Rev. Mater. Res. 41, 21-40.

Zhou, H., Lee, J., 2011. Nanoscale hydroxyapatite particles for bone tissue engineering, Acta Biomater. 7, 2769-2781.

Zhang, B.-B., Zheng, H., Ma, H.-W., Han, L-J., Zhang, H.-M., 2007. Phosphorus recovery from wastewater by synthetic tobermorite through seeded crystallization, Acta Petrol. Mineral. 26, 553-557.

Table 1

EDX analysis (at.%) from FE-SEM.

Treatment	C	O	Ca	P	Si	Cl	Na
$Wash_{Control}$	11.03 ±1.05	61.63 ±2.24	13.79 ±1.28	11.41 ±0.85	*a*	1.79 ±0.22	0.35 ±0.18
$Wash_{NaOH}$	11.72 ±2.21	64.20 ±4.31	13.93 ±2.77	9.66 ±1.43	0.49 ±0.09	*a*	*a*
$Wash_{EtOH}$	9.00 ±1.23	63.19 ±6.73	15.84 ±5.61	11.97 ±1.91	*a*	*a*	*a*

[a] Not detected

Legends for Figures

Fig. 1. SEM (a) and TEM (b) images of the product after washing with EtOH ($wash_{EtOH}$).

Fig. 2. Particle length distribution for product after the washing with EtOH ($wash_{EtOH}$).

Fig. 3. TEM image (a) and associated EDX spectrum of the measurement area (b) for the sample produced using $wash_{EtOH}$.

Fig. 4. XRD patterns of $wash_{NaOH}$ and $wash_{EtOH}$ after washing.

Fig. 5. High-resolution TEM image (a) and associated electron diffraction pattern (b) for the sample produced using $wash_{NaOH}$.

Fig. 6. FTIR spectrum of the sample after washing with EtOH ($wash_{EtOH}$).

Fig. 7. TGA of samples prepared by EtOH and NaOH washing ($wash_{NaOH}$ and $wash_{EtOH}$, respectively).

Fig. 8. XRD patterns of $wash_{NaOH}$ and $wash_{EtOH}$ after thermal treatment at 1200 °C.

Fig. 1.

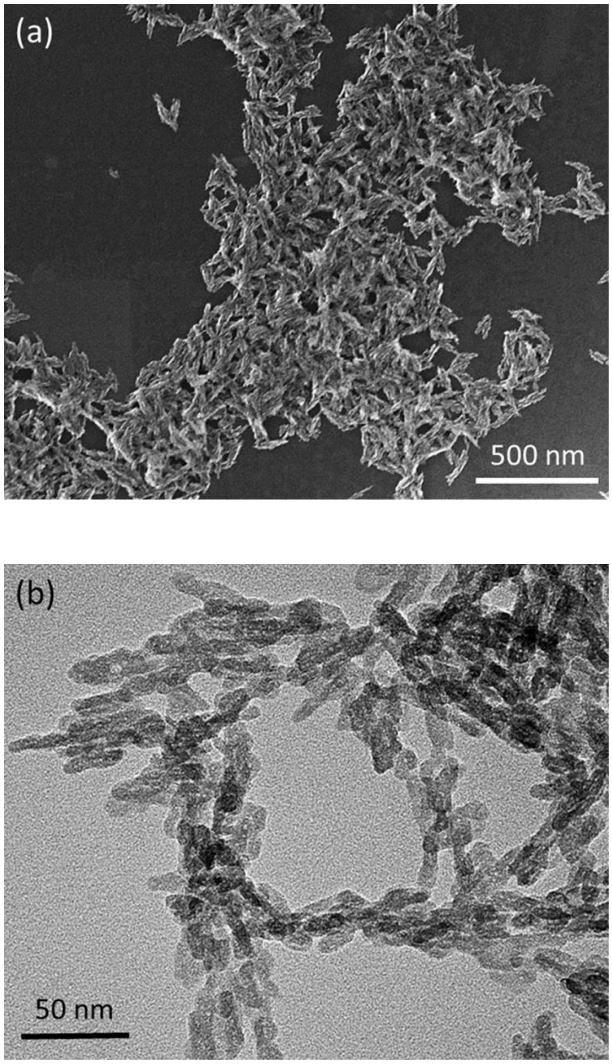

Fig. 2.

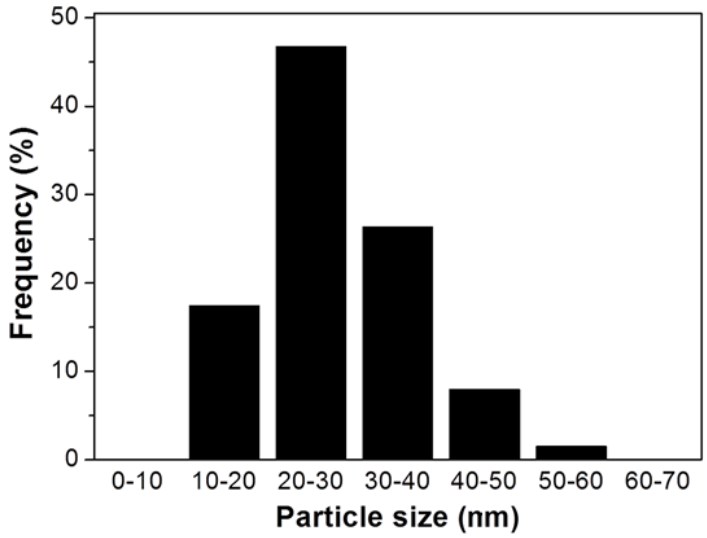
Frequency (%)
50
40
30
20
10
0
0-10
10-20
20-30
30-40
40-50
50-60
60-70
Particle size (nm)

Fig. 3

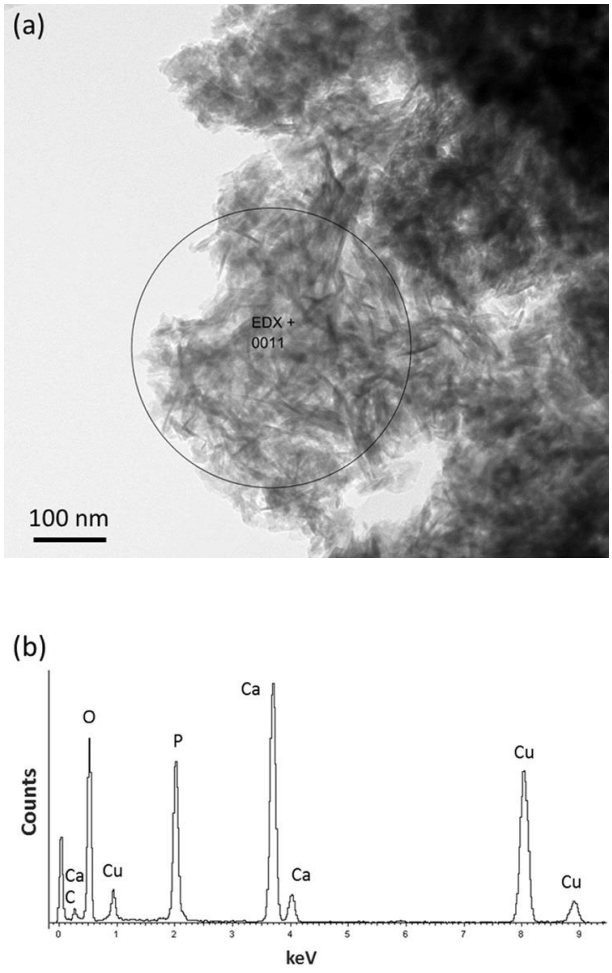

Fig. 4

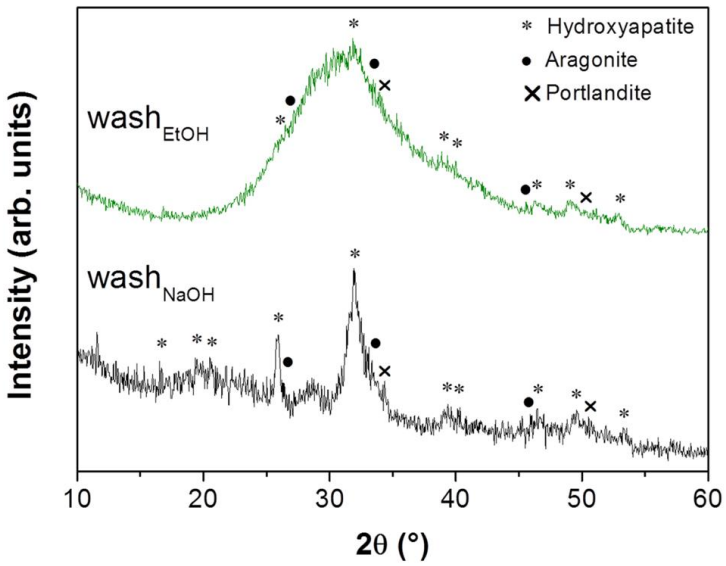
Hydroxyapatite
Aragonite
Portlandite
wash EtOH
wash NaOH
Intensity (arb. units)
10
20
30
40
50
60
2θ (°)

Fig. 5.

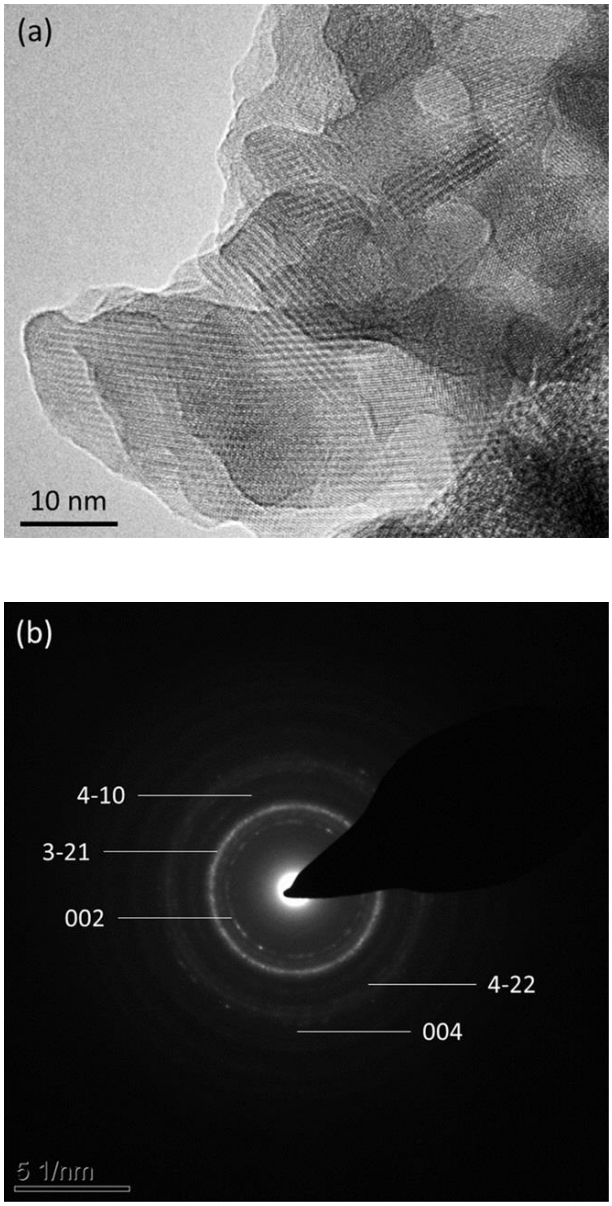

Fig. 6.

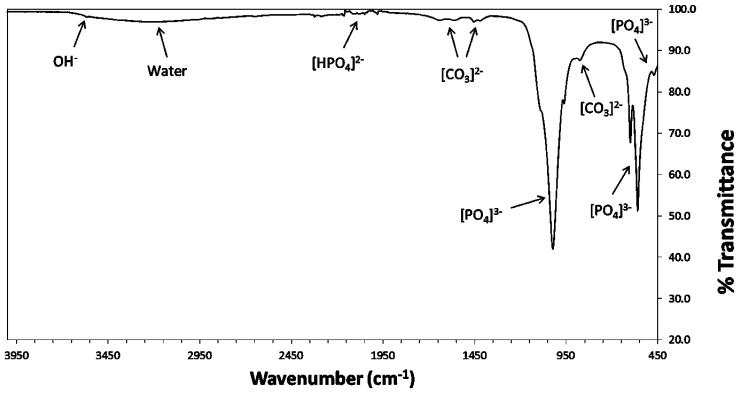
OH-
Water
[HPO4]2-
[CO3]2-
[PO4]3-
[CO3]2-
[PO4]3-
[PO4]3-
100.0
90.0
80.0
70.0
60.0
50.0
40.0
30.0
20.0
% Transmittance
3950
3450
2950
2450
1950
1450
950
450
Wavenumber (cm-1)

Fig. 7.

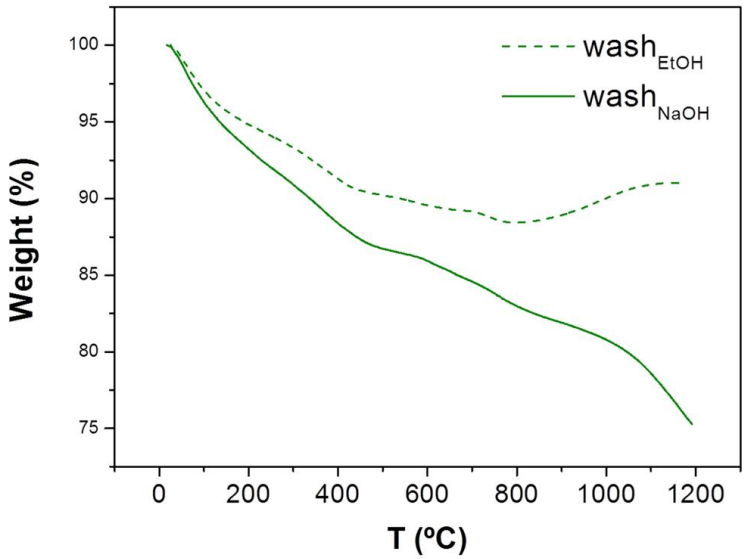
wash$_{EtOH}$
wash$_{NaOH}$
Weight (%)
T (ºC)
100
95
90
85
80
75
0
200
400
600
800
1000
1200

Fig. 8

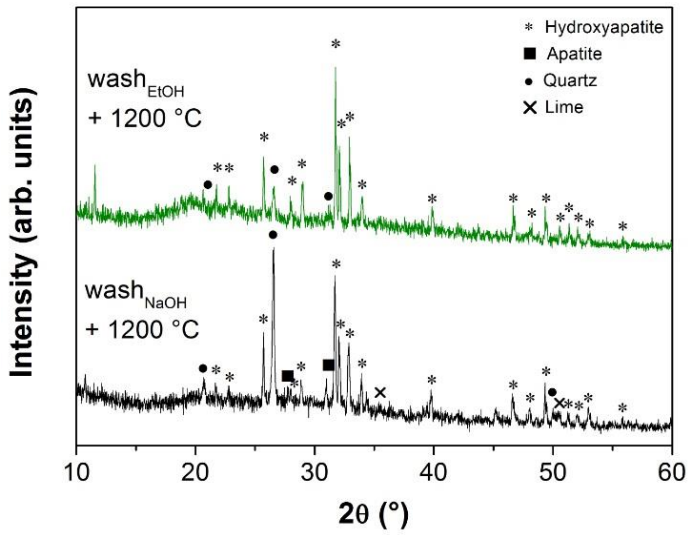
Hydroxyapatite
Apatite
Quartz
Lime
wash$_{EtOH}$
+ 1200 °C
wash$_{NaOH}$
+ 1200 °C
Intensity (arb. units)
10
20
30
40
50
60
2θ (°)

.